

# RSC Advances



This is an *Accepted Manuscript*, which has been through the Royal Society of Chemistry peer review process and has been accepted for publication.

*Accepted Manuscripts* are published online shortly after acceptance, before technical editing, formatting and proof reading. Using this free service, authors can make their results available to the community, in citable form, before we publish the edited article. This *Accepted Manuscript* will be replaced by the edited, formatted and paginated article as soon as this is available.

You can find more information about *Accepted Manuscripts* in the [Information for Authors](#).

Please note that technical editing may introduce minor changes to the text and/or graphics, which may alter content. The journal's standard [Terms & Conditions](#) and the [Ethical guidelines](#) still apply. In no event shall the Royal Society of Chemistry be held responsible for any errors or omissions in this *Accepted Manuscript* or any consequences arising from the use of any information it contains.

# ***In-situ* synthesis and photocatalytic performance of WO<sub>3</sub>/ZnWO<sub>4</sub> composite powders**

**Wen Li, Liyun Cao, Xingang Kong, Jianfeng Huang\*, Chunyan Yao, JieFei<sup>a</sup>,**

**Jiayin Li**

School of Materials Science & Engineering, Shaanxi University of Science and  
Technology, Xi'an 710021, China

**Abstract:** The WO<sub>3</sub>/ZnWO<sub>4</sub> composite powders were synthesized through an *in-situ* reaction process with tunnel structure K<sub>10</sub>W<sub>12</sub>O<sub>41</sub>·11H<sub>2</sub>O filiform crystallites used as precursor. At first, Zn<sup>2+</sup> ions was intercalated into K<sub>10</sub>W<sub>12</sub>O<sub>41</sub>·11H<sub>2</sub>O crystal by exchanging K<sup>+</sup> ions, then these Zn<sup>2+</sup>-exchanged samples were transformed into WO<sub>3</sub>/ZnWO<sub>4</sub> composite powders during heat-treatment. The formation reaction and structure of these samples were characterized by X-ray diffraction (XRD), field-emission scanning electron microscopy (FE-SEM), transmission electron microscopy (TEM) and energy dispersive x-ray spectrometer (EDS). Results showed that the WO<sub>3</sub>/ZnWO<sub>4</sub> composite powders consisted of WO<sub>3</sub> nanoparticles and ZnWO<sub>4</sub> nanorods. Photocatalytic experiments exhibited an excellent photocatalytic performance for the degradation of methylene blue (MB) and the degradation efficiency was about 95% after 70min under simulated sunlight.

**Keywords:** *in-situ* synthesis, WO<sub>3</sub>/ZnWO<sub>4</sub>, photocatalytic performance, heterojunctions

## **1 Introduction**

---

\*Corresponding author: Tel./fax: +86 029 86168802.

E-mail addresses: [huangjf@sust.edu.cn](mailto:huangjf@sust.edu.cn) (Jianfeng Huang);

*In-situ* synthesis process is a useful method for the preparation of function inorganic materials [1-3]. This process typically includes two steps: the first step is the preparation of a framework precursor with layered or tunnel, followed by the ions or molecules being inserted into the interlayer space by ion-exchange reaction. The second step is the transformation of the template-inserted precursor into a desired structure by the chemical method, such as solvothermal treatment, ion-exchange treatment and low temperature heat-treatment [4]. This method has been utilized for the synthesis and design of metal oxides and organic inorganic nanocomposites with controlled structure, morphology, and chemical composition [5].

Zinc tungstate ( $\text{ZnWO}_4$ ), as one of the important metal tungstates, has attracted wide interest due to its widespread and potential applications in various fields, such as scintillators, solid-state laser hosts, photocatalysts, gas and humidity sensors, optical fibers and electronic materials [6-14]. In the past decade, various morphological  $\text{ZnWO}_4$  nano/microstructures, such as rods, wires, hollow microspheres, hollow clusters and chrysanthemum-shape, have been synthesized through solid-state, precipitation, sol-gel, hydro/solvothermal and microwave routes [10-20]. In order to further enhance the photocatalytic properties and extend the applications of materials, their preparation with novel structures has attracted significant attention. Nowadays, several enhancement methods, such as the surface modification [21], organic/inorganic metal doping [22,23], and the combination with narrow band gap semiconductors [24], have been applied and tested to extend the light absorption spectrum from UV to visible light.

Generating heterojunctions is an effective method for photoelectron-hole separation to improve the photocatalytic efficiency of materials, such as  $\text{ZnO}/\text{ZnWO}_4/\text{WO}_3$ ,  $\text{Ag}-\text{AgBr}/\text{ZnWO}_4$ ,  $\text{WO}_3/\text{ZnO}$ ,  $\text{BiOBr}/\text{ZnWO}_4$ ,  $\text{TiO}_2/\text{ZnWO}_4\cdot\text{Yb}^{3+}$ ,  $\text{Tm}^{3+}$ ,  $\text{ZnO}/\text{ZnWO}_4$ ,  $\text{ZnWO}_4/\text{TiO}_2$  [25-31] are also

researched. Recently, the photoelectric properties of  $\text{WO}_3$  (2.8eV) related to solar energy conversion and the photocatalytic degradation are widely investigated [32, 33]. The result shows that  $\text{WO}_3$  has the high photoelectron catalytic degradation efficiency to azo dye pollutants [34] and high sensitivity to visible light [35]. However, the photoelectric properties and photocatalytic efficiency of  $\text{WO}_3$  require improvement in practical applications. Apart from  $\text{WO}_3$ , it is known that  $\text{ZnWO}_4$  (3.3eV) is a better photocatalyst with good photocatalytic effect and high quantum efficiency for degradation of environmental pollutants [36]. Among oxide semiconductors, combining  $\text{WO}_3$  with  $\text{ZnWO}_4$  has been very attractive in the achievement of efficient charge separation and photocatalytic activity improvement [31]. The other authors reported that the  $\text{WO}_3$  loaded into the  $\text{ZnWO}_4$  nanoparticles by microwave-solvothermal method and also discussed the photocatalytic degradation rate of the  $\text{WO}_3/\text{ZnWO}_4$  nanoparticles [37]. Therefore, a rapid screening technique utilizing a modified scanning electrochemical microscope has been used to screen photocatalysts and determine how metal doping affects its photoelectron chemical (PEC) properties by Bard research [38]. The electron transfer process between  $\text{WO}_3$  and  $\text{ZnWO}_4$  bilayer films also has been reported [39].

In this research, the  $\text{WO}_3/\text{ZnWO}_4$  composite powders are prepared by an *in-situ* synthesis reaction. In addition, the photocatalytic activities of these materials are discussed. To the best of our knowledge, such an approach towards the synthesis of  $\text{WO}_3/\text{ZnWO}_4$  composite powders has not been reported thus far.

## 2 Experimental

### 2.1 Preparation of $\text{K}_{10}\text{W}_{12}\text{O}_{41}\cdot 11\text{H}_2\text{O}$ precursor

The experimental procedure for preparing  $\text{K}_{10}\text{W}_{12}\text{O}_{41}\cdot 11\text{H}_2\text{O}$  nanocrystallites was as follows:

1g tungsten trioxide  $\text{WO}_3$  was dissolved in 30ml of 1.5mol/L-KOH solution (mole ratio of K/W $\approx$ 10:1), and then the mole ratio of K/W in the solution was controlled to 20:1 via adding KCl. The pH value of this solution was adjusted with HCl. Finally, the pH-adjusted solution was transferred into a Teflon-lined autoclave with an inner volume of 100ml, and maintained in an oven at 200°C for 12h. After the hydrothermal treatment, the products were filtered and washed with distilled water, then dried at room temperature.

## 2.2 Preparation of $\text{WO}_3/\text{ZnWO}_4$

A typical procedure (molar ratio of  $\text{WO}_3/\text{ZnWO}_4$  samples designed as 0.1:1) as follows: 0.5g of  $\text{K}_{10}\text{W}_{12}\text{O}_{41}\cdot 11\text{H}_2\text{O}$  samples were respectively put into 100ml of 0.5mol/L  $\text{Zn}(\text{CH}_3\text{COO})_2$ , then stirred and ion-exchanged for 12h at room temperature. The ion-exchange treatment was performed twice for the complete exchange. After ion-exchange, the products were filtered, washed with distilled water, and dried at room temperature. Thus the  $\text{Zn}^{2+}$ -exchanged samples were obtained. Finally, the  $\text{Zn}^{2+}$ -exchanged samples were heat-treated at 650°C for 2 h to obtain  $\text{WO}_3/\text{ZnWO}_4$  composite powders ( $\text{WO}_3/\text{ZnWO}_4\text{-HT}$ ). According to this method,  $\text{WO}_3/\text{ZnWO}_4$  samples with different molar ratios of 0.1:1, 0.2:1 and 0.3:1 were also obtained and denoted as 5%, 15% and 25%  $\text{WO}_3/\text{ZnWO}_4$  (mass ratio), respectively. In order to make a comparison, we synthesized the compound of the  $\text{WO}_3/\text{ZnWO}_4$  using the solid-state method ( $\text{WO}_3/\text{ZnWO}_4\text{-Solid}$ ). The mixtures consisting of 2.0g of the pure ammonium tungstate ( $(\text{NH}_4)_2\text{WO}_4$ ), 1.5g of the zinc nitrate ( $\text{Zn}(\text{NO}_3)_2\cdot 6\text{H}_2\text{O}$ ) and 1.25g of tungsten acid ( $\text{H}_2\text{WO}_4$ ) were put into the muffle furnace and heated at 600°C for 3 hours. Then the compounds of  $\text{WO}_3/\text{ZnWO}_4\text{-Solid}$  were obtained after being cooled in the air with the molar ratio of  $\text{ZnWO}_4$  and  $\text{WO}_3$  being 5/7.

## 2.3 Physical analysis

The crystal structure of the sample was investigated by a powder X-ray diffractometer (Shimadzu, Model XRD-6100) with Cu K $\alpha$  (1/40.15418 nm) radiation. The size and morphology of the particles were observed by scanning electron microscopy (SEM) (Hitachi, Model S-900). The element composition of the multi-layer coatings was analyzed with the energy dispersive spectroscopy (EDS). Transmission electron microscopy (TEM) observation and selected-area electron diffraction (SAED) were performed on a JEOL Model JEM-3010 system at 300 kV, and the powder sample was supported on a micro grid.

The photocatalytic performance of samples was evaluated by degradation of methylene blue (MB) under xenon lamp irradiation. In each experiment, 50 mg of samples were added into the solution (50 mL, 10 mg L<sup>-1</sup>). The suspensions were magnetically stirred in the dark for 60 min to ensure the establishment of an adsorption–desorption equilibrium. Then, the solution was exposed to the lamp irradiation under magnetic stirring. At different irradiation time intervals, 6 mL of the solution was collected by centrifugation. The concentration of the remnant dye in the collected solution was monitored by UV-vis spectroscopy (Unico UV-2600) each 5 or 10 min.

### 3 Result and discussion

#### 3.1 The K<sub>10</sub>W<sub>12</sub>O<sub>41</sub>·11H<sub>2</sub>O precursor

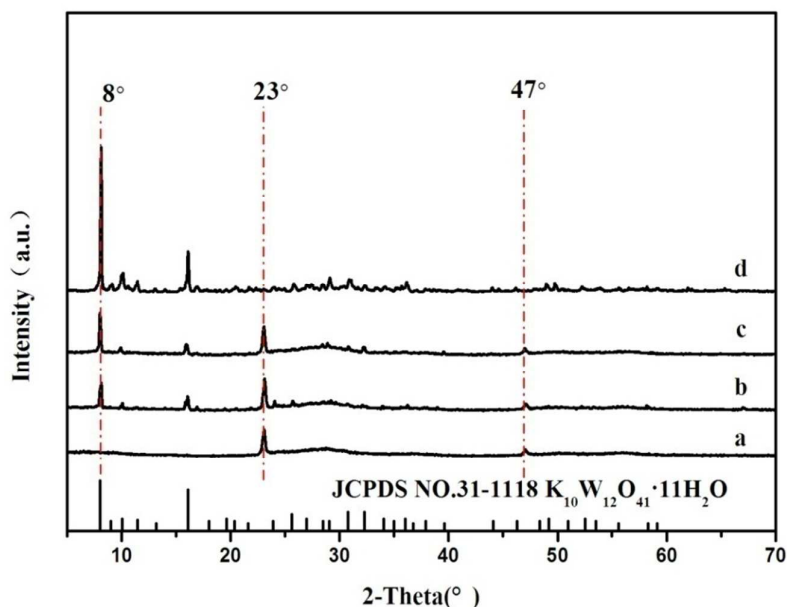


**Fig. 1 XRD patterns of samples obtained at the hydrothermal condition with different values, (a) pH=3, (b) pH=4, (c) pH=5, (d) pH=6**

$\text{WO}_3$  with KOH reacts easily under the condition of room temperature, forming soluble  $\text{K}_2\text{WO}_4$ , and then  $\text{K}_2\text{WO}_4$  is hydrothermally treated to transform into  $\text{K}_{10}\text{W}_{12}\text{O}_{41}\cdot 11\text{H}_2\text{O}$  in the acid system. Fig. 1 shows the XRD patterns of the potassium tungstate obtain in the K/W mole ratio of 20:1 under hydrothermal condition of  $200^\circ\text{C}$  for 12h. When the pH value is 3, the obtained sample respectively displays only two diffraction peaks at  $2\theta=23^\circ$  and  $47^\circ$  (Fig. 1a), but cannot be indexed in JCPDS File PDF card. Those peaks of this sample include the so-called  $\text{K}_2\text{W}_4\text{O}_{13}$  phase (JCPDS No. 20-0942) in literature [40], so it can be considered as the intermediate of potassium tungstate from amorphous phase to crystalline phase. When the pH value is 4, the  $\text{K}_{10}\text{W}_{12}\text{O}_{41}\cdot 11\text{H}_2\text{O}$  phase (JCPDS No. 31-1118) is formed, and two diffraction peaks at  $2\theta=23^\circ$  and  $47^\circ$  still exist in XRD pattern of product (Fig. 1b). In the XRD pattern of obtained sample after the hydrothermal reaction of pH=5 (Fig. 1c), it can be found clearly that the diffraction peaks intensity of  $\text{K}_{10}\text{W}_{12}\text{O}_{41}\cdot 11\text{H}_2\text{O}$  phase increase and the intensity of two diffraction peaks at  $2\theta=23^\circ$

and  $47^\circ$  decreases. Up to pH=6, two diffraction peaks at  $2\theta=23^\circ$  and  $47^\circ$  disappear, and the obtained samples only present a pure  $K_{10}W_{12}O_{41}\cdot 11H_2O$  phase (Fig. 1d). These results indicate that the potassium tungstate intermediate can be gradually transformed into  $K_{10}W_{12}O_{41}\cdot 11H_2O$  crystalline with the increase of pH value. In this hydrothermal reaction ( $10K^+ + 12WO_4^{2-} + 14H^+ + 4H_2O = K_{10}W_{12}O_{41}\cdot 11H_2O$ ), the increase of  $K^+$  ions concentration is conducive to the forward reaction according to the reaction equilibrium principle. So the  $K^+$  ions concentration is improved with KCl used as K source. When the K/W mole ratio is 20:1, the yield of products is the most. The above results indicate that the  $K_{10}W_{12}O_{41}\cdot 11H_2O$  phase can be synthesized via controlling pH value in the hydrothermal process of high K/W mole ratio.

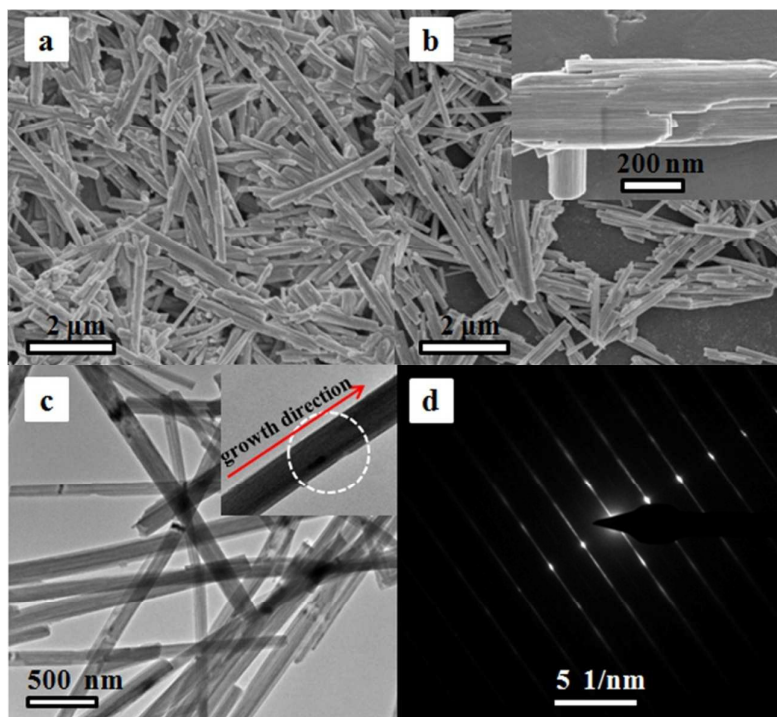


**Fig. 2** FE-SEM images (a, b), TEM image (c) and SEAD pattern (d) of samples obtained at the hydrothermal condition of 200 °C for 12h. (a) pH=3, (b, c, d) pH=6

Fig.2 shows the morphologies of samples obtained after the hydrothermal reaction at pH=3 and 6, respectively. It can be seen that the intermediate sample obtained at pH=3 exhibits a

rod-like shape with about 300nm in width and 3~10 $\mu$ m in length (Fig.2a). Nevertheless the pure  $K_{10}W_{12}O_{41} \cdot 11H_2O$  phase sample prepared at pH=6 also shows rod-like shape with about 300 nm in width and 3~10 $\mu$ m in length, and this nanorods contains a bunch of nanowires with about 10 nm in width which is observed in high magnification FE-SEM (Fig.2b). Similar to the FE-SEM results, the TEM images also show that the  $K_{10}W_{12}O_{41} \cdot 11H_2O$  phase sample has the 1D rod-like shape (Fig.2c). It is interesting that the  $K_{10}W_{12}O_{41} \cdot 11H_2O$  nanorod displays an individual SAED pattern (Fig.2d), in which the numerous satellite diffraction spots and the elongated lines perpendicular to the growing direction are observed (Fig.2d). The SAED pattern of  $K_{10}W_{12}O_{41} \cdot 11H_2O$  nanorod is similar to that of  $K_xWO_3$  reported by literatures [41, 42]. The emergence of this individual SAED pattern arises from the beam-like structure with nanowires self-assembling.

### 3.2 *In-situ* transformation reaction

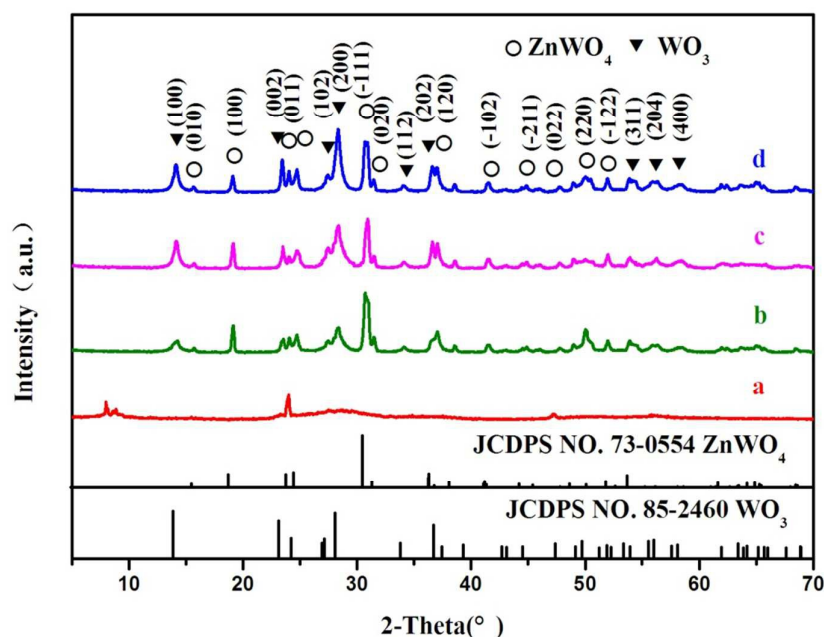
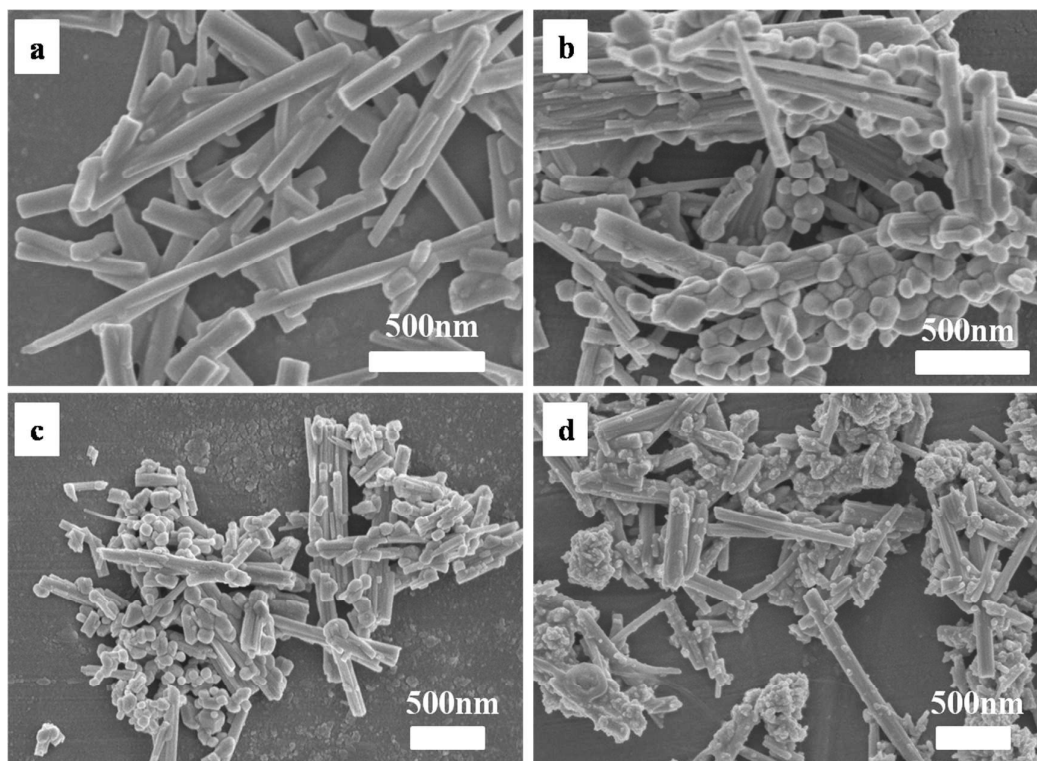


Fig.3 XRD patterns of (a) the  $Zn^{2+}$ -exchanged samples obtained in  $Zn(CH_3COO)_2$  solution

**and the samples of (b) 5wt% WO<sub>3</sub>/ZnWO<sub>4</sub>, (c)15wt% WO<sub>3</sub>/ZnWO<sub>4</sub> and (d) 25wt% WO<sub>3</sub>/ZnWO<sub>4</sub> obtained by heat-treating the Zn<sup>2+</sup>-exchanged samples from Zn(CH<sub>3</sub>COO)<sub>2</sub> solution**

Similar to the most metal oxides with tunnel structure, e.g. zeolites, tunnel structure manganese oxides [43, 44], layered tungstates of K<sub>2</sub>W<sub>3</sub>O<sub>10</sub>, K<sub>2</sub>W<sub>4</sub>O<sub>13</sub> [45], K<sup>+</sup> ions in the tunnel structure K<sub>10</sub>W<sub>12</sub>O<sub>41</sub>·11H<sub>2</sub>O can be exchanged with other cations by ion-exchange treatment. When the K<sub>10</sub>W<sub>12</sub>O<sub>41</sub>·11H<sub>2</sub>O precursor is treated by ion-exchange in 0.5 mol/L Zn(CH<sub>3</sub>COO)<sub>2</sub> aqueous solution, the Zn<sup>2+</sup>-exchanged samples are formed. Fig.3a shows that the crystallinity of Zn<sup>2+</sup>-exchanged samples is low, and the reason is that the Zn<sup>2+</sup> radius is smaller than the radius of K<sup>+</sup>, so the framework structure becomes loose. But the tunnel structure remains because of the existing characteristic peak at 2θ=10° nearby even if the intensity of the characteristic peak is weak. For the Fig.3b sample, the mixed phase of monoclinic ZnWO<sub>4</sub> (JCPDS No. 73-0554)/hexagonal WO<sub>3</sub> (JCPDS No. 85-2460) are formed after the heat-treatment of the Zn<sup>2+</sup>-exchanged sample obtained in Zn(CH<sub>3</sub>COO)<sub>2</sub> solution, and the crystallinity of this mixed phase was increased. With the increase of the WO<sub>3</sub> quality, the intensity of equivalent plane of the (100) (002) (200) are increased (Fig.3cd). No impurity peak is also found in the WO<sub>3</sub>/ZnWO<sub>4</sub> composites. This suggests that the photocatalyst is only composed of monoclinic ZnWO<sub>4</sub> and hexagonal WO<sub>3</sub>.



**Fig.4 SEM micrographs of the samples: (a) the  $Zn^{2+}$ -exchanged samples; (b) 5wt%  $WO_3/ZnWO_4$ ; (c) 15wt%  $WO_3/ZnWO_4$  and (d) 25wt%  $WO_3/ZnWO_4$**

The morphologies of  $Zn^{2+}$ -exchanged samples are shown in Fig.4a. The morphologies of  $Zn^{2+}$ -exchanged samples still maintain the rod-like structure of precursor, and the width or length have no change compared with the precursor  $K_{10}W_{12}O_{41} \cdot 11H_2O$ . After loading  $WO_3$ , many additional nanoparticles with 2-10nm in width are found adhered to the surface of the  $ZnWO_4$  nanorods (Fig.4b). With the increase of the  $WO_3$  quality, the phenomenon of the  $ZnWO_4$  surface adhered to the  $WO_3$  nanoparticles is decreased (Fig.4c). In the SEM micrograph of the 25wt%  $WO_3/ZnWO_4$  (Fig.4d), a smaller amount of  $WO_3$  particles adhere to the rod-shape  $ZnWO_4$  surface and a mass of  $WO_3$  nanoparticles agglomeration are appeared.

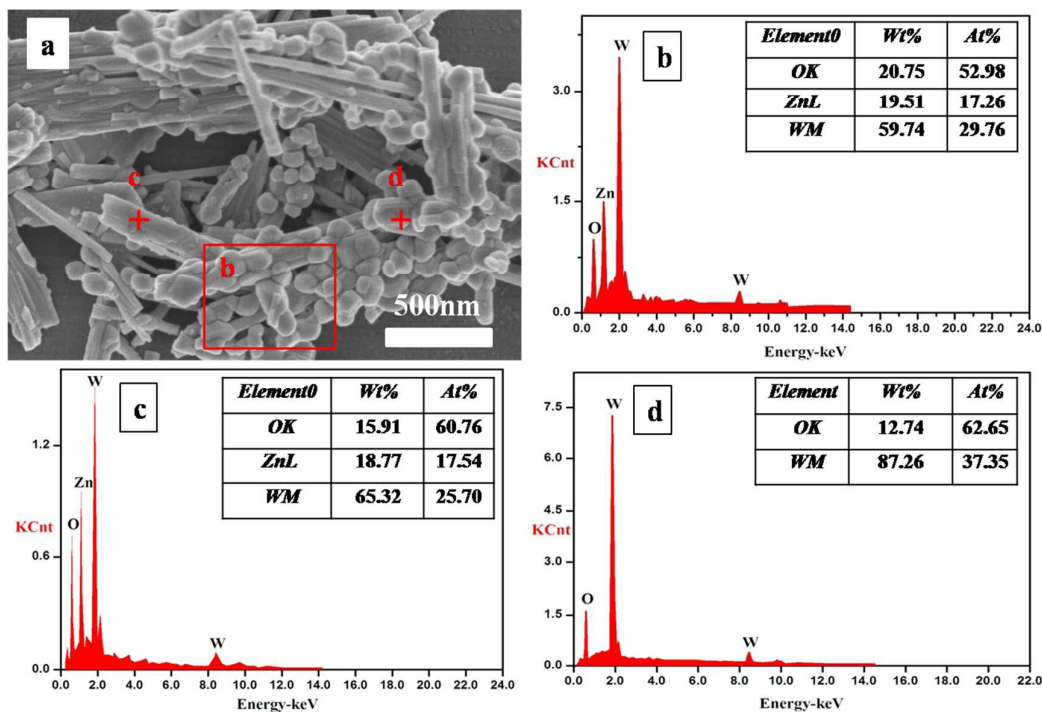


**Fig.5 SEM image (a) and EDS images (b)(c)(d)of the mixed phase of 5wt%WO<sub>3</sub>/ZnWO<sub>4</sub>-HT**

The element composition of the 5wt% WO<sub>3</sub>/ZnWO<sub>4</sub> samples is measured by the energy dispersive spectroscopy (EDS) analysis. From the area-scan EDS analysis (Fig.5b), the 5wt% WO<sub>3</sub>/ZnWO<sub>4</sub> composite powders are obtained. Zn element is detected in rod-like shape of WO<sub>3</sub>/ZnWO<sub>4</sub> samples and the element ratio of Zn atom and W atom is nearly 1:1(Fig.5c). Only W element and O element are detected in nanoparticles of WO<sub>3</sub>/ZnWO<sub>4</sub> samples and the element ratio of W atom and O atom is nearly 1:3(Fig.5d). The EDS analysis confirm that the sample consisted of nanorods ZnWO<sub>4</sub> and nanoparticles WO<sub>3</sub> which is consistent with the XRD results, and the morphology of nanorods ZnWO<sub>4</sub> depends on the morphology of nanorods K<sub>10</sub>W<sub>12</sub>O<sub>41</sub>·11H<sub>2</sub>O precursor sample.

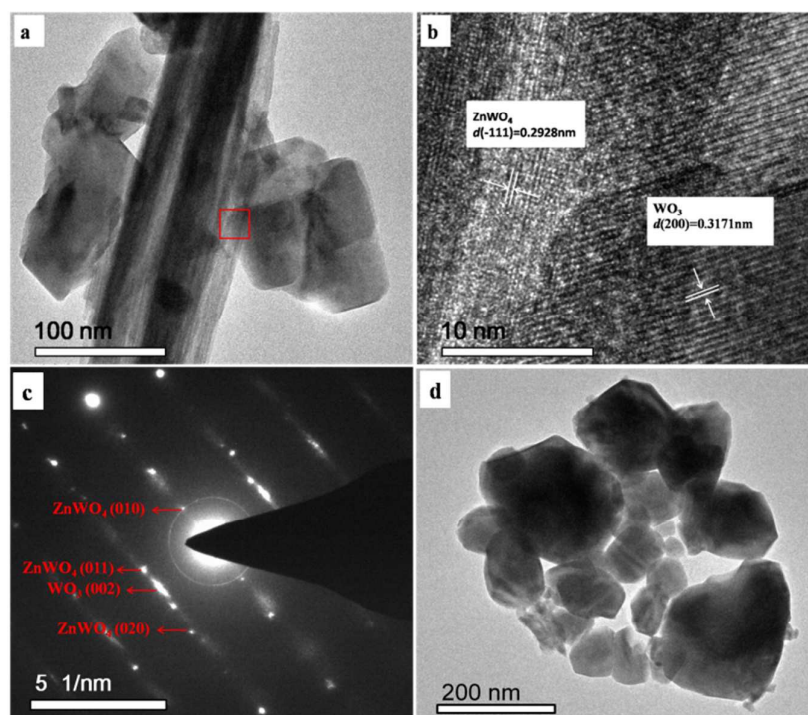


**Fig.6 TEM (a), HRTEM image (b) and SAED (c) of the 5wt%  $\text{WO}_3/\text{ZnWO}_4$  samples obtained by heat treating the  $\text{Zn}^{2+}$ -exchanged samples from  $\text{Zn}(\text{CH}_3\text{COO})_2$  solution, TEM (d) of the  $\text{WO}_3/\text{ZnWO}_4$  samples obtained by solid sintering method**

Corresponding to the SEM results, the TEM images also show that many additional irregular particles with 20-100nm in width are found adhered to the surface of the  $\text{ZnWO}_4$  nanorods in Fig.6 (a). By carefully measuring the lattice parameters with Digital Micrograph and comparing the data in JCPDS (Fig.6b), two different kinds of lattice fringes with spacing of 0.2928nm and 0.3171 nm are obtained. It can be sure that the lattice fringes with spacing of 0.2928nm belong to the (-111) crystallographic plane of monoclinic  $\text{ZnWO}_4$  (JCPDS No. 73-0554) and the lattice fringe with spacing of 0.3171 nm belongs to (200) plane of hexagonal  $\text{WO}_3$  (JCPDS No. 85-2460). So the nanorods could be  $\text{ZnWO}_4$  and the nanoparticles on the surface of the nanorods could be  $\text{WO}_3$ . The corresponding selected area electron diffraction (SAED) pattern is demonstrated in Fig.6c, which can be indexed to the  $\text{ZnWO}_4$  diffraction planes of (010), (020), (011) and  $\text{WO}_3$  diffraction

planes of (002), suggesting the composite is  $\text{WO}_3/\text{ZnWO}_4$ . From the TEM morphologies of Fig.6d, it is clearly discovered that the compound of  $\text{WO}_3/\text{ZnWO}_4$ -Solid is composed of different sizes of spherical particles, the average diameters of which are around 50-200nm. The size of samples obtained by solid sintering method is larger than that of samples by *in-situ* synthesis method. The smaller particle size contributed to the photocatalytic efficiency [46].

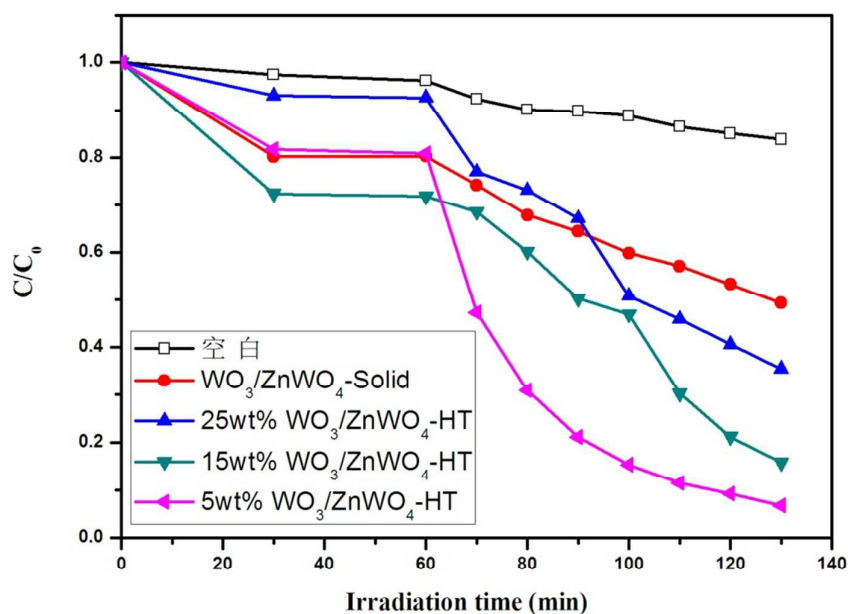


**Fig.7 Photocatalytic degradations of methylene blue (MB) under simulated sunlight irradiation using the as-prepared  $\text{WO}_3/\text{ZnWO}_4$ -Solid and  $\text{WO}_3/\text{ZnWO}_4$ -HT samples**

Fig. 7 shows the photocatalytic performance ( $C/C_0$ ) versus simulated sunlight irradiation time of samples for the degradation of methylene blue (MB). All samples show higher photocatalytic activity than  $\text{WO}_3/\text{ZnWO}_4$ -Solid dose and the 5%  $\text{WO}_3/\text{ZnWO}_4$ -HT shows the highest photocatalytic activity. The  $\text{WO}_3/\text{ZnWO}_4$ -Solid samples display the degradation efficiency of about 50% for MB after simulated sunlight irradiation for 70 min, however it takes about 10min for the 5wt%  $\text{WO}_3/\text{ZnWO}_4$ -HT sample to reach the degradation efficiency of about 50% for MB.

Ultimately, the degradations efficiency of MB are about 50%, 95%, 85% and 60%, respectively in  $\text{WO}_3/\text{ZnWO}_4$ -Solid, 5wt%  $\text{WO}_3/\text{ZnWO}_4$ -HT, 15wt%  $\text{WO}_3/\text{ZnWO}_4$ -HT and 25wt%  $\text{WO}_3/\text{ZnWO}_4$ -HT samples after 70min under simulated sunlight. It is found that the photocatalytic activities of  $\text{WO}_3/\text{ZnWO}_4$ -HT samples are superior to that of  $\text{WO}_3/\text{ZnWO}_4$ -Solid sample for the degradation of MB. The reason is that the smaller the particle size, the higher the photocatalytic efficiency. These small nanocrystals in  $\text{WO}_3/\text{ZnWO}_4$ -HT samples are generally beneficial for surface-based photocatalysis. More importantly, the existence of the heterojunction in the  $\text{WO}_3/\text{ZnWO}_4$ -HT composite powders improve the separation of the electrons and holes generated by the photons, so the synergetic effect may occur in the grain boundary between  $\text{ZnWO}_4$  nanocrystal and  $\text{WO}_3$  nanocrystal in hetero-nanostructures [47,48]. In addition, the MB degradations efficiency of 5wt%  $\text{WO}_3/\text{ZnWO}_4$ -HT is superior to the 25wt%  $\text{WO}_3/\text{ZnWO}_4$ -HT. This reason is the  $\text{WO}_3$  nanoparticles agglomeration are appeared and led to a reduction in the number of heterojunction in  $\text{WO}_3/\text{ZnWO}_4$  composite.

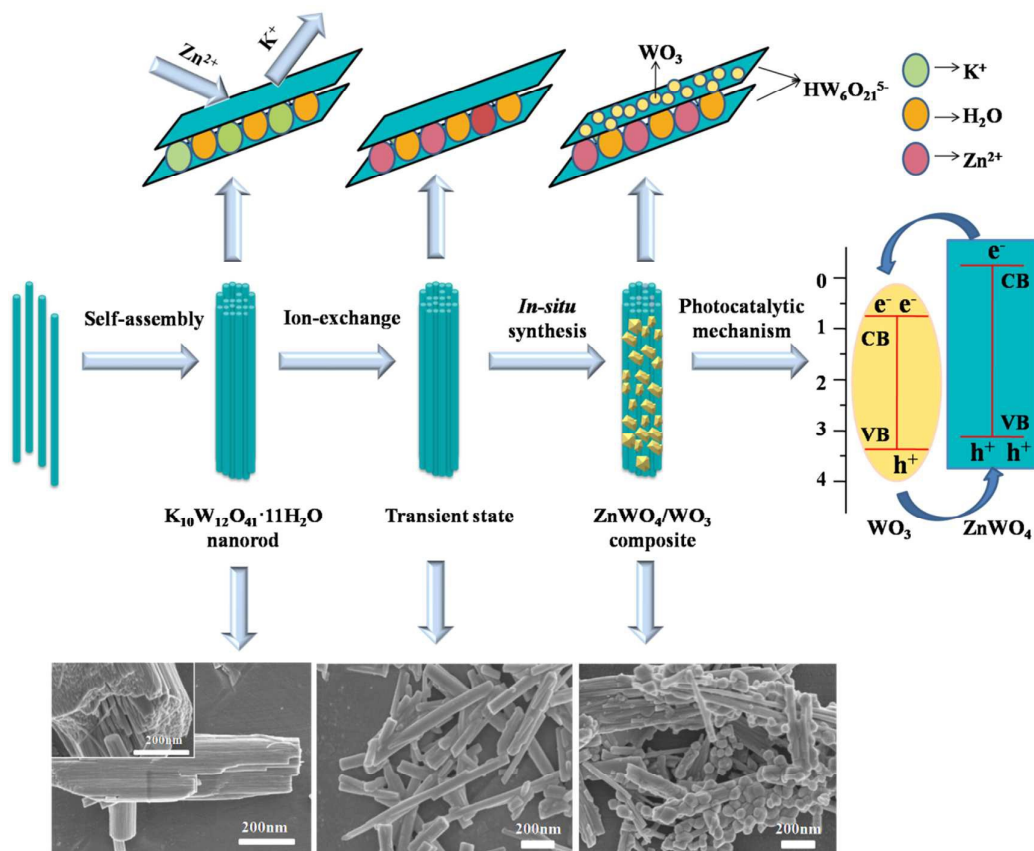


**Fig.8 Formation mechanism and photocatalytic mechanism of the 1D rod-like  $\text{WO}_3/\text{ZnWO}_4$  composite from the layered  $\text{K}_{10}\text{W}_{12}\text{O}_{41}\cdot 11\text{H}_2\text{O}$  precursor**

On the basis of the above results, we propose a formation mechanism and photocatalytic mechanism of the 1D rod-like  $\text{WO}_3/\text{ZnWO}_4$  composite from layered  $\text{K}_{10}\text{W}_{12}\text{O}_{41}\cdot 11\text{H}_2\text{O}$  precursor, as shown in Fig.8. The mechanism of formation of the 1D rod-like  $\text{WO}_3/\text{ZnWO}_4$  composite consists mainly of two processes, ion-exchange and *in situ* crystallization. Firstly, the  $\text{Zn}^{2+}$  ions come in contact with the  $\text{HW}_6\text{O}_{21}^{5-}$  layers of the  $\text{K}_{10}\text{W}_{12}\text{O}_{41}\cdot 11\text{H}_2\text{O}$  phase or intercalate with the  $\text{HW}_6\text{O}_{21}^{5-}$  interlayer via  $\text{K}^+/\text{Zn}^{2+}$  ion exchange, and then straightaway *in situ* react with  $\text{HW}_6\text{O}_{21}^{5-}$  layers to generate the  $\text{ZnWO}_4$  nanocrystal. Finally, when the unreacted  $\text{K}_{10}\text{W}_{12}\text{O}_{41}\cdot 11\text{H}_2\text{O}$  phase within the composite is thoroughly depleted, the  $\text{ZnWO}_4$  no longer obtains, and the rest of the tungsten source irreversibly transform into  $\text{WO}_3$  during the heat treatment. The mechanism described above suggests that the biggest advantage of *in situ* synthesis method is can make the

WO<sub>3</sub>/ZnWO<sub>4</sub> product keep its nanorods shape of original base K<sub>10</sub>W<sub>12</sub>O<sub>41</sub>·11H<sub>2</sub>O material [49]. The optical band gap energy of ZnWO<sub>4</sub> and WO<sub>3</sub> is 3.3eV and 2.8eV, respectively. The band gaps of the two semiconductors match well with each other. Under simulated sunlight irradiation, both the ZnWO<sub>4</sub> and WO<sub>3</sub> are excited by absorbing photons, and then electron-hole pairs are produced. The WO<sub>3</sub> acts as electron-accepting semiconductor. Photogenerated electrons transfer from the conduction band (CB) of ZnWO<sub>4</sub> to that of WO<sub>3</sub>. Simultaneously, holes shift from the valence band (VB) of WO<sub>3</sub> to that of ZnWO<sub>4</sub>. The effectively separation of photogenerated electrons and holes can be enhanced, which result in higher photocatalytic performance [50-52].

#### 4 Conclusions

The WO<sub>3</sub>/ZnWO<sub>4</sub> composites powders were successfully synthesized by *in-situ* reaction process with the tunnel structure K<sub>10</sub>W<sub>12</sub>O<sub>41</sub>·11H<sub>2</sub>O rod-like crystallites used as precursor. Zn<sup>2+</sup> ions were intercalated into K<sub>10</sub>W<sub>12</sub>O<sub>41</sub>·11H<sub>2</sub>O crystal by exchanging K<sup>+</sup> ions and then these Zn<sup>2+</sup>-exchanged samples were transformed into WO<sub>3</sub>/ZnWO<sub>4</sub> during heat-treatment. Photocatalytic experiments showed that 5wt% WO<sub>3</sub>/ZnWO<sub>4</sub> composites powders have excellent photocatalytic performance for the degradation of methylene blue (MB) with the degradation efficiency being about 95% after 70min under simulated sunlight irradiation. The *in-situ* reaction process is an efficient method for designing and preparing other new types of nanostructures or hetero-nanostructures functional materials

#### Acknowledgments

Innovation Team Assistance Foundation of Shaanxi Province (2013KCT-06), Innovation Team Assistance Foundation of Shaanxi University of Science and Technology (No.TD12-05), National Natural Science Foundation of China (No. 51472152).

## References

- [1] X.G. Kong, Y. Ishikawa, K. Shinagawa, Q. Feng, *JAm Ceram Soc*, 2011, 11, 3716-3721.
- [2] X.G. Kong, D.W. Hu, P. Wen, Q. Feng, *Dalt T*, 2013, 21, 7699-7709.
- [3] S. Kundu, K. Wang, D. Huitink, *Langmuir*, 2009, 25, 10146-10152.
- [4] X.G. Kong, D. Hu, Y. Ishikawa, Y. Tanaka, *Chem Mater*, 2011, 17, 3978-3986.
- [5] X.G. Kong, Z.L. Guo, P.H. Wen, L.Y. Cao, *RSC Adv*, 2014, 100, 56637-56644.
- [6] S.J. Chen, J.H. Zhou, X.T. Chen, *Chem Phys Lett*, 2003, 1, 185-190.
- [7] S. Lin, J. Chen, X. Weng, *Mater Res Bull*, 2009, 5, 1102-1105.
- [8] H. Fu, J.Lin, L. Zhang, *Appl Catal A: Gen*, 2006, 306, 58-67.
- [9] L.H. Thomas, C. Wales, L. Zhao, *Cryst Growth Des*, 2011, 5, 1450-1452.
- [10] M.B.Nazari, M. Shariati, M.R. Eslami, *Mechanika*, 2010, 84, 20-27.
- [11] Z. Amouzegar, R. Naghizadeh, H.R. Rezaie, M. Ghahari, *Ceram Int*, 2015, 7, 8352-8359.
- [12] X. Zhao, Y. Zhu, *Environ Sci Technol*, 2006, 10, 3367-3372.
- [13] J. Lin, J. Lin, Y. Zhu, *Inorg Chem*, 2007, 20, 8372-8378.
- [14] X. Zhao, W. Yao, Y. Wu, *J Solid State Chem*, 2006, 8, 2562-2570.
- [15] M. Wang, Y. Tang, T. Sun, *Cryst Eng Comm*, 2014, 48, 11035-11041.
- [16] T.Montini, V.Gombac, A. Hameed, *Chem Phys Lett*, 2010, 1, 113-119.
- [17] B. Liu, S.H. Yu, L. Li, *J Phys Chem B*, 2004, 9, 2788-2792.
- [18] K.M. Garadkar, L.A. Ghule, K.B. Sapnar, *Mater Res Bull*, 2013, 3, 1105-1109.
- [19] W. Zhao, X. Song, G. Chen, *J Mater sci*, 2009, 12, 3082-3087.
- [20] J. Huang, L. Gao, *J Am Ceram Soc*, 2006, 12, 3877-3880.
- [21] K. Peng, A. Lu, R. Zhang, *Adv Funct Mater*, 2008, 19, 3026-3035.
- [22] X.H. Wang, J.G. Li, H. Kamiyama, *J Phys Chem B*, 2006, 13, 6804-6809..
- [23] G. Liu, Y. Zhao, C. Sun, *Angew Chem Int Edit*, 2008, 24, 4516-4520.
- [24] Y. Bessekhoad, N. Chaoui, M. Trzpit, *J Photoch Photobio A*, 2006, 1, 218-224..
- [25] Y. Wang, L. Cai, Y. Li, *Physica E*, 2010, 1, 503-509.
- [26] K. Li, J. Xue, Y. Zhang, *Appl Surf Sci*, 2014, 320, 1-9.
- [27] Y. Liu, H. He, J. Li, *RSC Adv*, 2015, 58, 46928-46934.
- [28] X.C. Song, W.T. Li, W.Z. Huang, *Mater Chem Phys*, 2015, 160, 251-256.

- [29] K. Feng, S. Huang, Z. Lou, Dalton T, 2015, 30, 13681-13687.
- [30] A. Dodd, A. McKinley, T. Tsuzuki, M. Saunders, J Eur Ceram Soc, 2009, 29, 139-144.
- [31] W. Wang, W.F. Bai, B. Shen, J.W. Zhai, Ceram Int, 2015, 41, 435-440.
- [32] I. Shiyankovskaya, M. Hepel, J Electrochem Soc, 1999, 1, 243-249.
- [33] R. Solarska, C. Santato, C. Jorand-Sartoretti, J applelectrochem, 2005, 7, 715-721.
- [34] M. Hepel, S. Hazelton, Electrochim Acta, 2005, 25, 5278-5291..
- [35] G. Waldner, A. Brüger, N.S. Gaikwad, Chemosphere, 2007, 4, 779-784.
- [36] J. Lin, J. Lin, Y. Zhu, Inorgchem, 2007, 20, 8372-8378.
- [37] Y. Keereeta, S. Thongtem, T. Thongtem, Powder Technol, 2015, 284, 85-94.
- [38] K.C. Leonard, K.M. Nam, H.C. Lee, J Phys Chem C, 2013, 117, 15901-15910.
- [39] H. Wei, D. Ding, X. Yan, Electrochim Acta, 2014, 132, 58-66.
- [40] A.S. Koster, F. Kools, G.D. Rieck, Acta Crystallogr B, 1969, 9, 1704-1708.
- [41] C. Guo, S. Yin, L. Huang, ACS appl materinter, 2011, 7, 2794-2799.
- [42] S. Jia, H. Zheng, H. Sang, ACS appl materinter, 2013, 20, 10346-10351.
- [43] Q. Feng, H. Kanoh, K. Ooi, J Mater Chem, 1999, 2, 319-333.
- [44] P. Misaelides, Micropor Mesopor Mat, 2011, 1, 15-18.
- [45] A. Martinez-de La Cruz, L.G.C. Torres, Ceram Int, 2008, 7, 1779-1782.
- [46] Z. Jiang, Y. Tang, Q. Tai, et al, Adv Energy Mater, 2013, 10, 1368-1380.
- [47] W. Lu, J. Xiang, B.P. Timko, P Natl Acad Sci USA, 2005, 29, 10046-10051.
- [48] M. Pirhashemi, A. Habibi-Yangjeh, Ceram Int, 2015, 10, 14383-14393.
- [49] X.G. Kong, Z.L. Guo, C.B. Zeng, J Mater Chem A, 2015, 3, 18127-18135.
- [50] S. Kundu, K. Wang, H. Liang, J Phys Chem C, 2009, 113, 18570-18577.
- [51] S. Kundu, J Mater Chem C, 2013, 1, 831-842.
- [52] S. Kundu, S.K. Ghosh, M. Mandal, New J Chem, 2003, 27, 656-662.